Selective laser melting of titanium alloy with 50 wt% tantalum: Microstructure and mechanical properties

Swee Leong Sing [a, b], Wai Yee Yeong [a, b, *], Florencia Edith Wiria [a, c]

[a] SIMTech-NTU Joint Laboratory (3D Additive Manufacturing), Nanyang Technological University, HW3-01-01, 65A Nanyang Drive, Singapore 637333, Singapore
[b] Singapore Centre for 3D Printing, School of Mechanical & Aerospace Engineering, Nanyang Technological University, HW1-01-05, 2A Nanyang Link, Singapore 637372, Singapore
[c] Singapore Institute of Manufacturing Technology, 71 Nanyang Drive, Singapore 638075, Singapore

ARTICLE INFO

ABSTRACT

In this study, selective laser melting (SLM) was used to fabricate samples of titanium—tantalum (TiTa) alloy comprising 50 wt% of each element. Based on observation from scanning electron microscopy, as-fabricated samples comprised of randomly dispersed pure tantalum particles in a TiTa matrix. The microstructure exhibited equiaxed grains of β titanium and tantalum in random orientations, determined by combination of field emission scanning electron microscopy, electron back scatter diffraction and X-ray diffraction. The resulting samples have ultimate tensile strength of 924.64 ± 9.06 MPa and elastic modulus of 75.77 ± 4.04 GPa. The TiTa alloy produced can be a potential material for biomedical applications due to its high strength to modulus ratio, as compared to Ti6Al4V and commercially pure titanium.

© 2015 Elsevier B.V. All rights reserved.

1. Introduction

Selective laser melting (SLM) is a form of additive manufacturing, or more commonly known as 3D printing, technique that uses a laser power source to fuse powder materials to form functionally parts directly based on computer aided design (CAD) files. The details of the process have been described in various works [1–6]. The widely known established materials for SLM are stainless steel, tool steel, Ti6Al4V and AlSi10Mg. Recent researches focus on expanding the material library for this process [7–11], process simulations [12,13] as well as characterizing and improving the mechanical properties of established materials [14–16].

The capability of SLM to process powder mixtures has opened up new and exciting material research opportunities. Several works have been reported on the production of several types of new powder mixture processed by SLM [17–21]. Titanium alloys are superior biomedical materials due to their excellent combination of biocompatibility, corrosion resistance and mechanical properties [6]. Extensive research have been conducted on SLM of titanium alloys. In particular, Ti6Al4V [4,22–26] and Ti6Al7Nb [27–29] are well characterized due to their wide applications. Both of these titanium alloys are more commonly used in biomedical applications. However, safety concerns were raised recently on these materials as they contain aluminum which can cause neurological problems in human body after long term usage, and/or vanadium which is cytotoxic [30–33]. There is a need for development of new titanium alloys that are free of these toxic elements. Furthermore, there is also a need to develop materials of reduced modulus to avoid mismatch in modulus between the implant and adjacent bones. Clinical investigations indicate that the mismatch will result in insufficient load transfer from the artificial implants to neighboring bones. This leads to bone resorption and potential loosening of the implant. This effect is known as "stress shielding" [31].

Tantalum is an excellent choice for alloying with titanium for biomedical applications due to its' high biocompatibility, corrosion resistance and good mechanical properties. Furthermore, titanium—tantalum (TiTa) alloys are promising materials for such applications because of high strength to density ratio and low cost

---

* Corresponding author. SIMTech-NTU Joint Laboratory (3D Additive Manufacturing), Nanyang Technological University, HW3-01-01, 65A Nanyang Drive, Singapore 637333, Singapore.
E-mail addresses: sing0011@e.ntu.edu.sg (S.L. Sing), wyyeong@ntu.edu.sg (W.Y. Yeong), florencia@simtech.a-star.edu.sg (F.E. Wiria).

[34]. Alloying elements in titanium can be classified into 3 groups: (1) stabilizer for the α phase, (2) stabilizer for β phase or (3) have no observable effect on the phase [21]. Depending on the specific application of the materials, the different phases of titanium provide wide array of properties. In particular, tantalum is a β stabilizing element for titanium alloy. β titanium alloys display superior properties with lower modulus compared to the commonly used alloys in the biomedical field, such as stainless steels and cobalt-chromium alloys [18] and Ti6Al4V which is an α + β titanium alloy [30].

The lower modulus is desirable in applications in the biomedical field as it minimizes the adverse effect of stress shielding. Despite the advantages, not much research has been done on β titanium using SLM. Vrancken *et al.* managed to create a novel metallic composite comprising of β titanium matrix and unmelted molybdenum particles using SLM [21]. In their work, a mixture of Ti6Al4V pre-alloyed powder and molybdenum powder were used. The resulting material has a Young's modulus of 73 ± 1 GPa, yield strength of 858 ± 16 MPa, ultimate tensile strength of 919 ± 10 MPa and elongation of 20.1 ± 2.0%.

TiTa alloys are still not widely adopted in applications. The main reason is the difficulties in combining these two metals as they have great difference in melting point and density [30]. In particular, tantalum has a density of 16.6 g/cm^3 which is about 4 times of the density of commercially pure titanium. This could lead to inhomogeneity during the formation of alloys as the difference in density can lead to segregation of elements in the alloys.

In this paper, TiTa parts were manufactured via SLM. The feedstock used is a mixture of commercially pure titanium and tantalum powders with equal weight percentages. Microstructure of the SLM produced TiTa parts, such as phase formation, grain size and grain morphology, will be discussed. The product's mechanical properties such as elastic modulus, ultimate tensile strength, yield strength and microhardness, will be evaluated and benchmarked against SLM produced Ti6Al4V and commercially pure titanium parts.

2. Experimental procedure

2.1. Powder preparation

Both commercially pure titanium and tantalum powders are produced by gas atomization. The commercially pure titanium powder (Grade 2 ASTM B348, LPW Technology Ltd, United Kingdom) is spherical in shape and has particle size with average size of 43.5 μm. The tantalum powder (Singapore Demand Planner Ltd, Singapore) is irregular in shape and has average particle size of

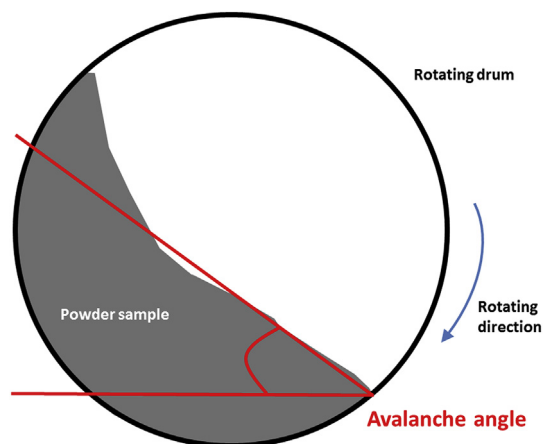**Fig. 2.** Schematic of the avalanche angle measured in flowability test.

44 μm. The morphologies of the commercially pure titanium and tantalum powders are shown in Fig. 1.

The two powders were mixed in weight ratio of 1:1 and then spun at a rate of 60 rpm for 12 h using a tumbler mixer (Inversina 2L, Bioengineering AG). The mixed powder density was measured using gas displacement pycnometry system (AccuPyc II 1340, Micromeritics).

Flowability tests were conducted on the commercially pure titanium, tantalum and TiTa powders using the revolution method (Revolution Powder Analyzer, Mercury Scientific Inc.). In this test, a tapped volume of 100 cm^3 of powder was measured by freely filling a cup that was gently tapped until no more powder could fit in. Excess powder was removed using a sharp edge. The powder was then placed inside the cylindrical drum with transparent glass sides. The drum was set to rotate at 0.3 rpm and a digital camera was used to monitor the flow behavior of the powder. Due to the drum rotation, the powder would be carried up along the side of the drum until it could not support its weight, forming avalanches. The avalanche angle was computed by measuring the angle where the powder was at maximum position before the start of the avalanche. Lower avalanche angles are indicative of better flowability of powders. The avalanche angle is illustrated in Fig. 2.

2.2. Selective laser melting

Fabrication of all the samples was carried out on a SLM 250HL machine (SLM Solutions Group AG, Germany). The SLM machine is equipped with a Gaussian beam fiber laser with maximum power
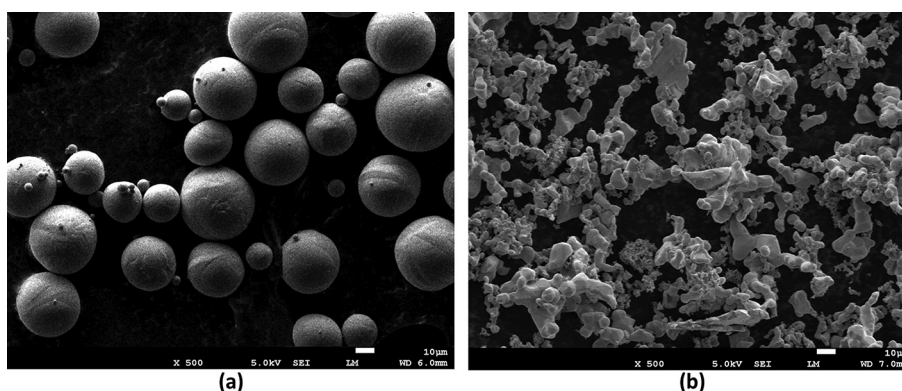

Fig. 1. FESEM image of (a) commercially pure titanium powder and (b) tantalum powder.

of 400 W and a focal diameter of 80 μm. All processing occurred in an argon environment with less than 0.05% oxygen to prevent oxidation and degradation of the material during the process [35]. Sectorial, also known as island or chessboard, scanning as shown in Fig. 3 was used. This scanning strategy has been reported to minimize thermal stresses formed during the process [36,37] The process parameters are shown in Table 1. The parameters are chosen after a series of experiments to obtain the highest relative density of parts fabricated from the powder mixture using SLM.

2.3. Metallographic characterization

The SLM samples were subjected to standard metallographic procedure which is grinding with 320, 800 and 1200 SiC papers and then polished by diamond suspensions of 9, 3 and 1 μm sizes. The samples were then etched with Kroll's reagent (10 mL of HF, 30 mL of HNO$_3$ and 50 mL of water, ASTM E407) for 20 s. The microstructure study was conducted using field emission scanning electron microscopy (FESEM, JEOL JSM7600), X-ray diffraction (XRD, Empyrean from Panalytical) and electron back scattered diffraction (EBSD, Oxford Instruments Nordlys). The grain size distribution was measured from the EBSD results using postprocessing software, HKL CHANNEL5 (Oxford Instruments).

2.4. Mechanical characterization

Tensile coupons with gauge length of 40 mm (based on ASTM E8) were produced using wire-cut discharge machining (EDM) from SLM fabricated blocks, as shown in Fig. 4.

Tensile test (Instron Static Tester Series 5569) was conducted with 50 kN and strain rate of 1 mm/min. Tensile test loading direction was perpendicular to the build direction, i.e. along the xy-plane. A schematic of build orientation during the SLM process is shown in Fig. 5.

The build direction is along the z-axis for all test samples.

The microhardness test of the material was carried out using Vickers hardness test (DuraScan, Struers) on the xy-plane and yz-
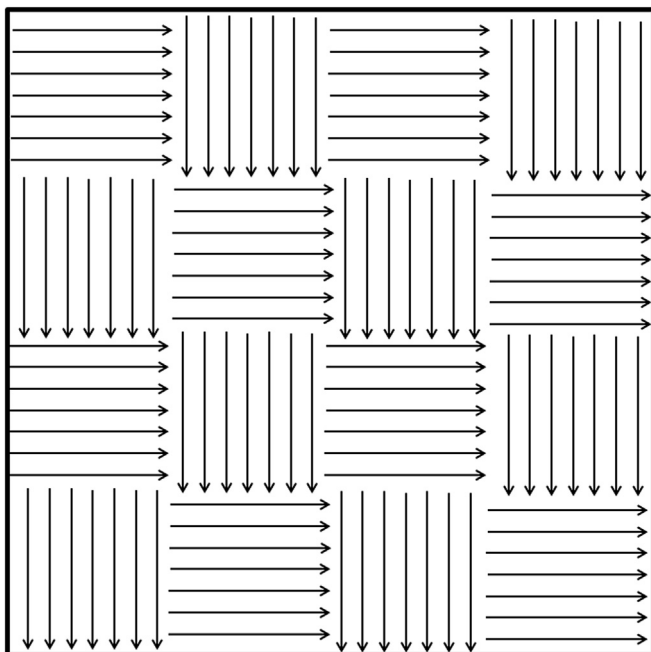
Table 1
SLM processing parameters for TiTa.

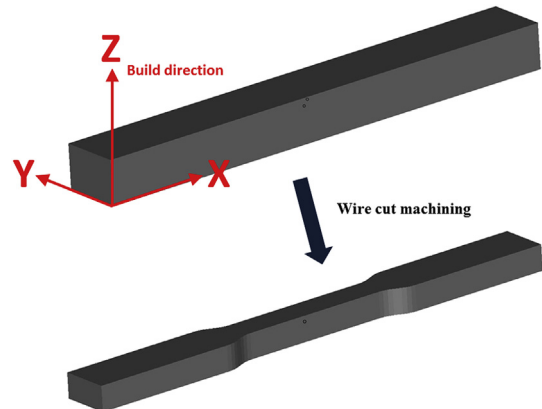| Process parameters	
Laser power (W)	360
Laser scan speed (mm/s)	400
Layer thickness (μm)	50
Hatch spacing (mm)	0.125
Remelting	No
Island length (mm)	5 × 5
Island overlap (mm)	1
Relative density (%)	99.9

Fig. 4. Schematic of producing tensile coupons from blocks fabricated by SLM.
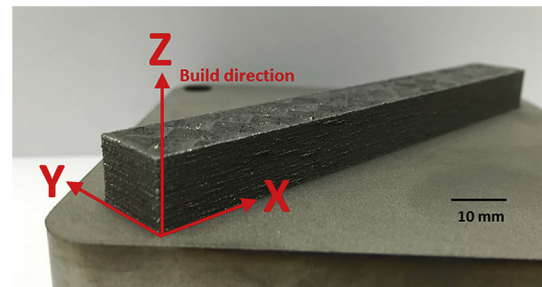

Fig. 5. Build orientation of blocks fabricated using SLM.

plane with a load of 100 g and a loading time of 15 s.

3. Results and discussion

3.1. Powder characterization

The mixing procedure was effective in mixing these two types of powder together, as shown in Fig. 6. The titanium powder remained spherical after the mixing, which is important for the flowability of the powder mixture. The TiTa mixed powder composition was ascertained by inductive coupled plasma atomic emission spectroscopy (ICP-AES) and energy-dispersive x-ray spectroscopy (EDS). The results are tabulated in Table 2.

There are advantages in mixing commercially pure titanium and tantalum powders, as follows:

1) Flowability is a key concern in SLM, as uniform powder deposition is required for production of parts with high relative density. Spherical powder is ideally desired. However, the tantalum powder has non-spherical shape, as its high melting

Fig. 3. Chessboard strategy used in SLM.
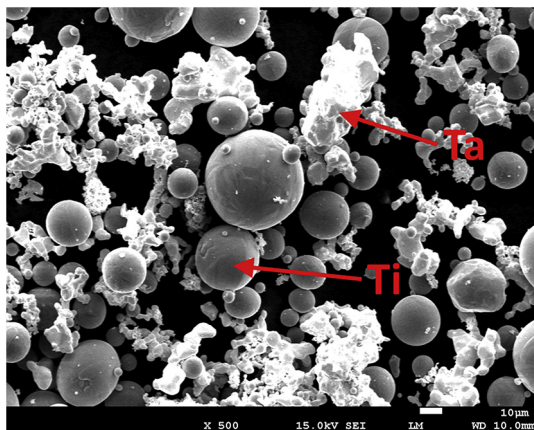
Fig. 6. Ti + Ta powder mixture. The spherical powder is Ti and the irregular powder is Ta.

Table 2
Chemical composition of TiTa alloy.

Element	Nominal (wt%)	ICP-AES (wt%)	EDS (wt%)
Ti	50	51.27	55.74 ± 1.06
Ta	50	48.19	44.26 ± 1.06

point of 3020 °C restricts the production of spherical powder economically. Hence, the overall flowability is improved by mixing the tantalum powder with spherical commercially pure titanium powder. The spherical titanium particles roll easier during powder depositions and acts as a medium by pushing the tantalum particles along.

Flowability can be indicated by the avalanche angle of the powders. Table 3 shows the average avalanche angle of commercially pure titanium, tantalum and TiTa mixed powders for 150 avalanches.

The results show that the TiTa mixed powder has better flowability compared to the non-spherical tantalum powder. However, the blended powder flowability is still lower compared to the commercially pure titanium powder. Nonetheless, the improvement in flowability is sufficient for powder deposition and subsequent fabrication by SLM as shown in the experiments conducted in this study.

2) Tantalum has a high density of 16.6 g/cm³. The powder volume increases for a specific weight of the powder mixture by mixing tantalum powder with commercially pure titanium powder, as compared to processing pure tantalum powder, due to the lower density of commercially pure titanium (4.51 g/cm³). This lower the production cost of processing in SLM as larger powder volume allows fabrication of larger parts.

Physical properties of commercially pure titanium and tantalum are summarized in Table 4.

Table 3
Avalanche angle of commercially pure titanium, tantalum and TiTa powders.

Material	Avalanche angle (deg) n = 150
cpTi	44.65 ± 3.19
Ta	56.51 ± 5.88
Ti–Ta	52.54 ± 4.25

Table 4
Physical properties of pure titanium and tantalum powders.

Materials	Density (g/cm³)	Melting point (°C)
Ti	4.51	1650
Ta	16.69	3020

Table 5
Theoretical and measured densities of TiTa powder.

| Material	Theoretical density (g/cm³)	Measured density (g/cm³)
TiTa	7.10	7.0835 ± 0.0035

The theoretical and measured densities of TiTa mixed powder is tabulated in Table 5.

3.2. XRD phase analysis

It is observed from Fig. 7 that the peaks in the TiTa mixed powder pattern corresponds to the respective peaks of the tantalum powder and commercially pure titanium powder.

The XRD spectrums of SLM produced TiTa samples are also shown in Fig. 7. After the SLM process, the respective diffraction peaks of titanium and tantalum can still be observed. However, only the peaks corresponding to the β phase are observed. Pure titanium has a hexagonal close packed (HCP) structure, i.e. α phase, at ambient temperature. At temperature greater than 883 °C, it exists as a body centered cubic structure (BCC), i.e. β phase. The β phase becomes stable at temperatures lower than 883 °C when β stabilizers are added and can be maintained in the metastable state at ambient temperature. The BCC structure stability depends on the extent of alloying elements. The amount of β stabilizer required to retain purely β phase at ambient temperature depends on the Molybdenum Equivalency [21], an empirical rule derived from analysis of binary titanium alloys. In general, approximately 10 wt% of molybdenum is required to stabilize the β phase during quenching [38]. During SLM, the parts undergo rapid cooling which is similar to rapid quenching. Molybdenum Equivalence is given by

$$Mo_{eq} = 1.0Mo + 0.67V + 0.44W - 0.28Nb + 0.22Ta + 1.6Cr$$
$$+ \cdots - 1.0Al$$

$$(1)$$
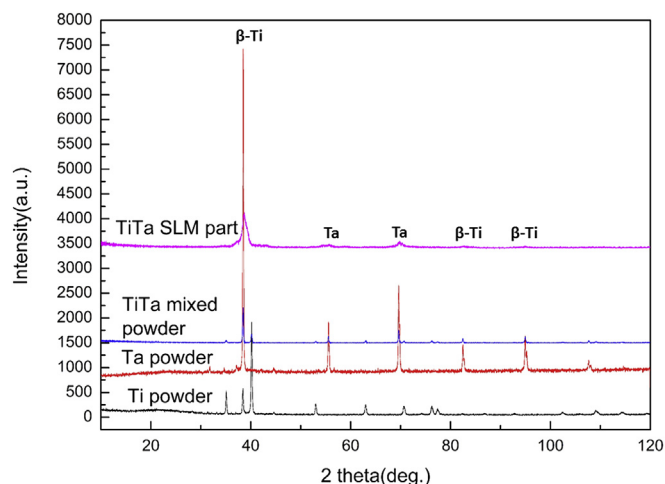
Fig. 7. XRD patterns of commercially pure titanium, tantalum, TiTa powders and SLM produced TiTa.

Based on the Molybdenum Equivalence, the TiTa alloy formed has a Mo_{eq} of 11, which is more than 10 but less than the critical value of 25. It signifies that the resulting β titanium from SLM of the mixture of commercially pure titanium and tantalum powders is metastable. β titanium and tantalum have similar atomic radii (approximately 0.2 nm) and both have bcc structures with lattice parameter of approximately 332 pm, their XRD peaks coincide. They also share the same peaks as β(Ti,Ta) solid solution [39].

The addition of tantalum in the alloy suppresses the transformation of β phase to the α′ phase due to the β stabilizing effect. This was achieved by decreasing the critical cooling rate to retain β phase and lowering of the martensitic start temperature. Coupled with the rapid solidification during SLM process, SLM produced TiTa exhibits single β phase microstructure and not α + β despite being metastable. Previous studies have also shown the preference of formation and growth of β phase over α phase at large undercooling [40]. Metastable β titanium alloys are advantageous as their mechanical properties can be tailored [41]. This implies that the SLM produced TiTa parts can be heat treated to obtain various combinations of mechanical properties for different applications.

3.3. Microstructure of titanium—tantalum parts

The resulting microstructures of the SLM samples in xy-plane and yz-plane are shown in Fig. 8.

The SLM produced samples consist of TiTa solid solution matrix with unmelted tantalum particles. The applied energy density during SLM is sufficient to fully melt the titanium powder but some of the larger tantalum particles only melted partially due to the higher melting point of tantalum. The composition of the TiTa matrix was determined to be 50.74 ± 0.82 wt% of titanium and 49.26 ± 0.82 wt% of tantalum. The composition of the TiTa matrix is consistent throughout, even near the boundary of the unmelted tantalum. The consistency of the composition shows that the diffusion of melted tantalum into the matrix is not obstructed by the partial melting. The relatively large two phase (liquid + solid) field in the binary titanium-tantalum phase diagram also shows the difficulty in melting the two materials together. This resulted in the tantalum particles in TiTa matrix microstructure shown in Fig. 8.

Equiaxed β grains can be observed, as shown in Fig. 8. Due to the isomorphous β stability effect of tantalum, no α phase is formed during the rapid cooling in SLM. The equiaxed β grains arise due to the melting of scan tracks and layers that resulted in temperature about the β transus. Partial remelting between adjacent scan tracks resulted in melt tracks formation that is larger than the laser spot size of 80 μm. Furthermore, there was also remelting of previous layer due to penetration depth of the laser larger than the layer
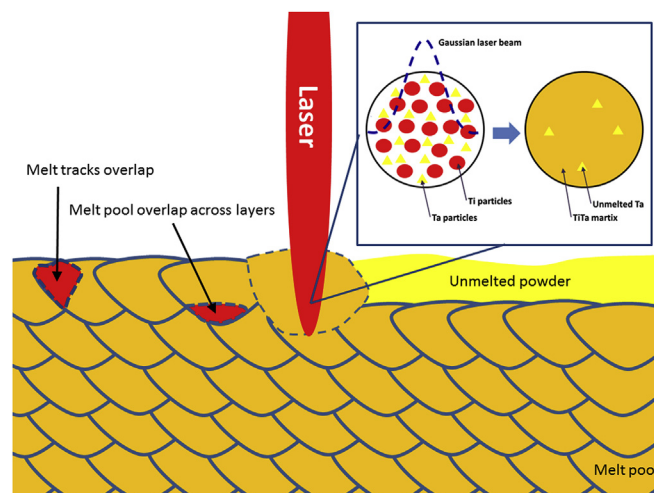
Fig. 9. Schematic of overlapping melt tracks and melt pools during SLM.

thickness of 50 μm. This allows growth of the grains that are parallel, inclined or perpendicular to the build direction in various sizes. This indicates that the grains grow from multiple locations in the melt pool boundary A schematic showing the overlapping of melt tracks and melt pools is shown in Fig 9.

In addition, the main driving force in the molten pools of SLM process is the convection applied by the combination of surface tension gradient, viscous shear stress and buoyancy forces [42]. During solidification of the molten pool in SLM, the laser beam moves forward and thermal energy is quickly dissipated to the substrate or previous solidified layer due to the higher thermal conductivity of solid compared to the surrounding powder [21,42]. This results in temperature gradients within the melt pool. The temperature gradients result in chemical potential gradient of solute elements and different directions of liquid flow. These phenomena result in random orientation of the grains formed due to multiple mass flow directions. Furthermore, during SLM, laser scanning is performed line-by-line, followed by layer-by-layer. These influenced the grain formation in multiple directions, as observed in Fig. 8, due to corresponding thermal flows. The directions of the resulting grains are determined using EBSD, as shown in Fig. 10.

Similar to SEM images, the EBSD images shows equiaxed β grains developed and grew within each layer in multiple directions. The random grain orientations results in anisotropic microstructure without any preferred grain orientation, despite the rapid
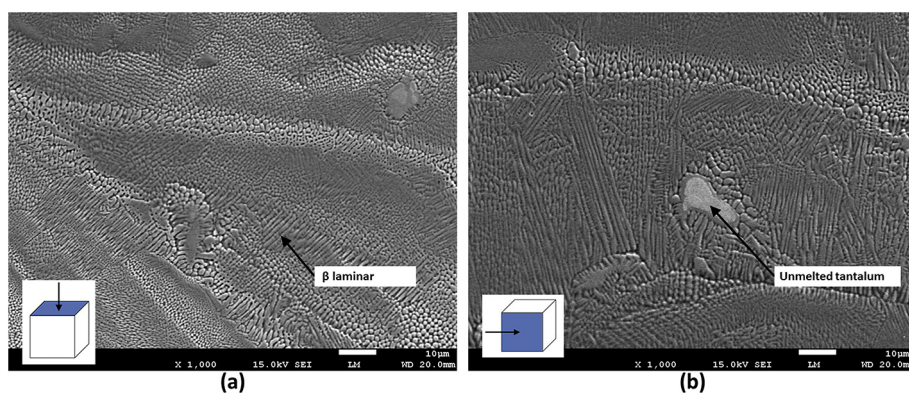
Fig. 8. FESEM micrograph of SLM produced TiTa samples (a) xy and (b) yz plane.
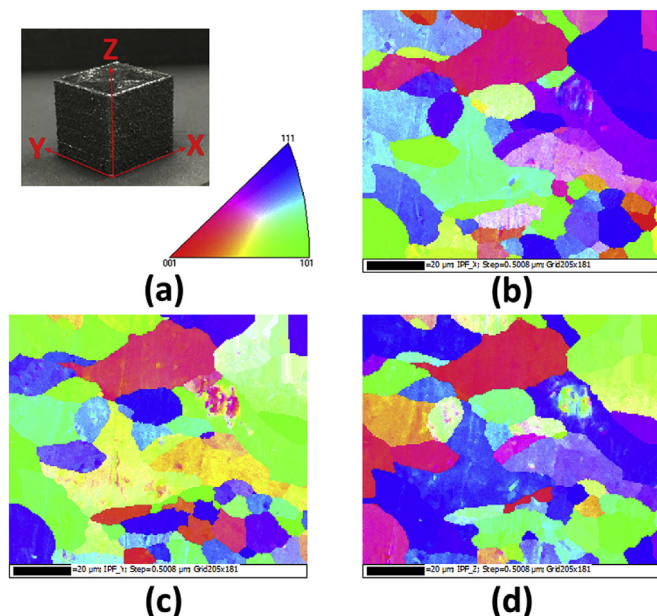
Fig. 10. EBSD maps showing different orientation of grains (a) specimen and grain orientations (b) xy (c) yz and (d) xz planes with respect to build orientation.
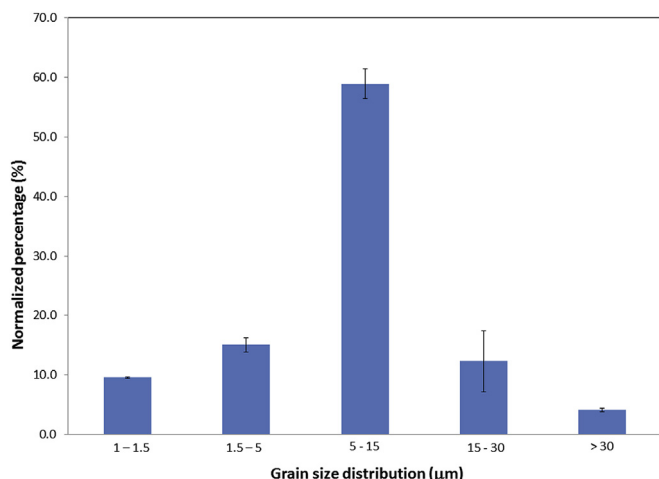

Fig. 11. Grain size distribution of SLM produced TiTa samples.

solidification rate. Furthermore, due to the scanning strategy which involves the laser beam moving backwards and forwards, the grain structures produced consist of grains in random orientations.

From Fig. 11, it is observed that the grain size of the samples is generally smaller than the laser spot size of 80 μm. This observation implied that there were multiple nucleus sites for grain formation along one single melt track. The grains formed were orientated in various orientations due to the temperature gradients that existed in multiple orientations.

The grain size in SLM produced TiTa samples has an average value of 10.20 ± 7.68 μm and the grain size distribution is shown in Fig. 11. The difference in grain size can be attributed to the difference in thermal conductivity of titanium (21.9 W/mK) and tantalum (57.5 W/mK). When the grain nucleate in proximity to the unmelted tantalum, heat is conducted away quicker due to the higher thermal conductivity of tantalum, this results in smaller grains formed as the solidification rate is higher.

In solidification process, the temperature gradient in the liquid phase, G and the growth of the interface, or solidification rate, R are the two main factors that affect the grain morphology. From literature, a high G and low R (i.e. high G/R ratio) will result in columnar growth, while low G and high R (i.e. low G/R ratio) result in equiaxed growth [43]. From the titanium-tantalum phase diagram, the temperature range between liquidus and solidus is approximately 300 °C for titanium with 50 wt% tantalum which allows for solidification to occur within short time periods during SLM. Furthermore, rapid solidification occurs during SLM inherently, hence, R is high during SLM. The sectorial scan strategy used in this study has shorter scan tracks which tend to produce lower temperature gradients (low G) [44]. The low G/R ratio resulting in formation of the equiaxed grains in SLM produced TiTa.

Within each of the equiaxed grains, laminar β phase substructures with directionality can be observed. The substructure surrounds the unmelted tantalum particles grow in direction parallel to the surface of the particles due to tantalum having higher thermal conductivity compared to the titanium−tantalum solid solution, which results in higher G surrounding the tantalum particles as heat is dissipated away from the liquid phase faster along the tantalum particles. When the melt tracks overlap, G is also increased due to remelting. This results in formation of laminar substructures in the solidified TiTa. The formation of these laminar substructure with directionality is due to the Gaussian laser heat source which non uniform power distribution and fluctuating energy output [45]. This results in multiple temperature gradients of different direction within the melt pool. Coupled with the multiple nucleation sites in the melt pool and differences in thermal conductivity between the liquid, solid and powder, directionality in the substructures occurs. A schematic showing the formation of laminar substructures is shown in Fig 12.

In comparison, SLM produced commercially pure titanium consist of primary α phase while SLM produced Ti6Al4V samples consist of α′ phase. The phase transformation in the SLM produced materials is determined by solidification behaviors of the molten pool with complete liquid formation, including the liquid flow, solidification rate and thermal history [46]. Heating and cooling over the beta transus temperature leads to complete re-nucleation of phases. The difference in microstructure between these three materials is captured by XRD analysis as shown in Fig. 13. The resulting microstructures of commercially pure titanium and Ti6Al4V samples are also shown in Fig. 14 and Fig. 15 respectively.
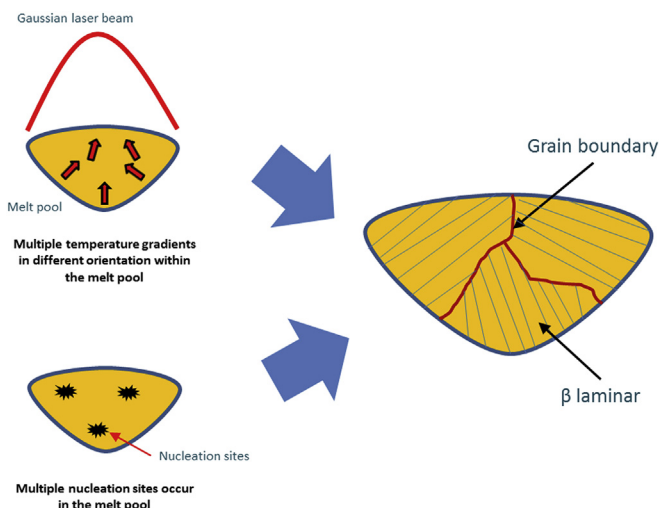

Fig. 12. Formation of β laminar substructure in equiaxed grains in SLM produced TiTa.
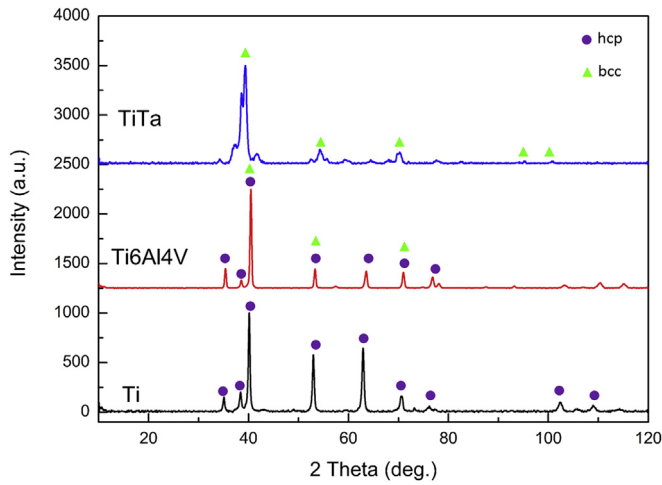
Fig. 13. XRD patterns of SLM produced commercially pure titanium, Ti6Al4V and TiTa.

Standard XRD peaks corresponding to hexagonal closed pack (HCP) structure was detected for the commercially pure titanium and Ti6Al4V samples. The HCP structure is determined to be α phase for commercially pure titanium samples from the FESEM images which shows the microstructure consisting of a mixture of acicular and platelet α. The platelet α is formed when rapid cooling occurred during SLM from temperature above the beta transus of 883 °C, allowing the transformation of β into α phase. However, in Ti6Al4V samples, the HCP structure is determined to be α′ phase from the FESEM images which shows complete martensitic microstructure. Martensitic laths transformed from prior β grain boundaries and fill the grains. Furthermore, the XRD pattern of Ti6Al4V samples indicates presence of a HCP phase with lattice parameters a = 0.2944 nm and c = 0.4678 which is in agreement with the lattice parameter values given for the α′ phase (a = 0.29313 nm and c = 0.46813 nm) in literature [26].

The materials in SLM undergo very high cooling rates during the process. However, these cooling rates vary due to the differences in
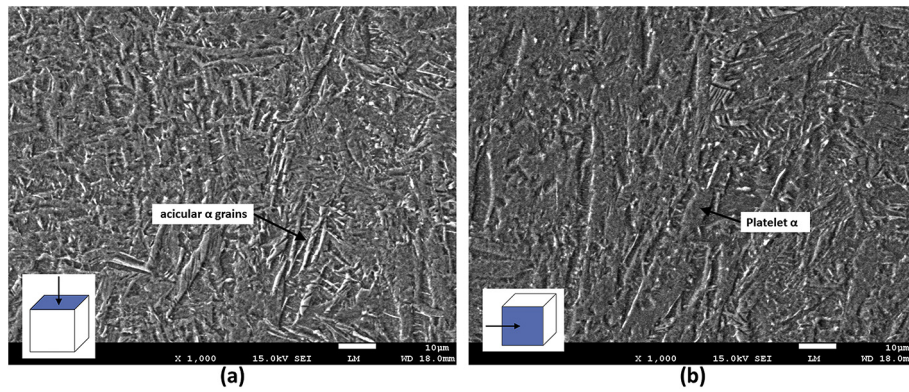
Fig. 14. FESEM micrograph of SLM produced commercially pure titanium samples (a) xy and (b) yz plane.
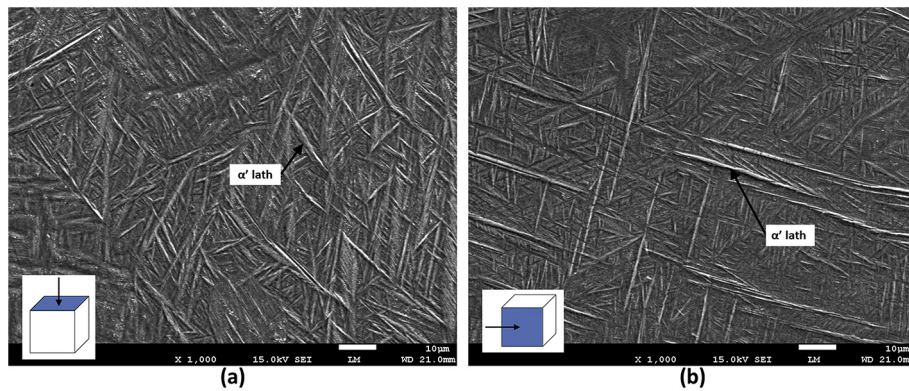
Fig. 15. FESEM micrograph of SLM produced Ti6Al4V samples (a) xy and (b) yz plane.

Table 6
Tensile properties of SLM produced TiTa, Ti6Al4V and commercially pure titanium samples (n = 5).

Material	Young's modulus (GPa)	Ultimate tensile strength (MPa)	Yield strength (MPa)	Elongation (%)
TiTa	75.77 ± 4.04	924.64 ± 9.06	882.77 ± 19.60	11.72 ± 1.13
Ti6Al4V	131.51 ± 16.40	1165.69 ± 107.25	1055.59 ± 63.63	6.10 ± 2.57
cpTi	111.59 ± 2.65	703.05 ± 16.22	619.57 ± 20.25	5.19 ± 0.32
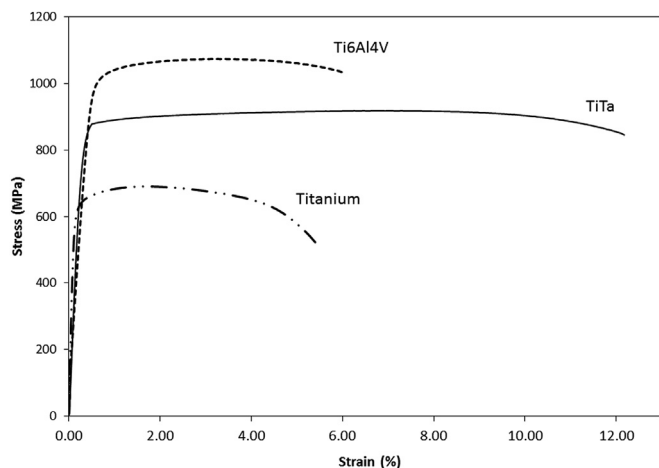
Fig. 16. Stress-strain curves of SLM produced TiTa, commercially pure titanium and Ti6Al4V specimens.

Table 7
Microhardness of SLM produced TiTa, Ti6Al4V and commercially pure titanium samples.

Material	xy-plane (HV)	yz-plane (HV)
TiTa	284.5 ± 11.06	282.7 ± 9.76
Ti6Al4V	383.16 ± 10.62	386.83 ± 8.73
cpTi	213.4 ± 10.29	217.4 ± 3.67

physical properties of the materials. In addition, the difference in composition of commercially pure titanium, Ti6Al4V (with $\alpha + \beta$ stabilizers) and TiTa (with β stabilizer) results in varying beta

transus. The difference in cooling rates and beta transus lead to different microstructure formation in the three materials.

3.4. Mechanical properties

The tensile properties of SLM produced commercially pure titanium, Ti6Al4V and TiTa are shown in Table 6. All tensile coupons and tests were conducted in-house, using the same machines and test equipment, with same parameters stated in previous section. The corresponding typical stress–strain curves are plotted in Fig. 16.

The Young's modulus of SLM produced TiTa is the lowest. The elastic modulus of an alloy is mainly determined by the modulus and volume fractions of the constitution phases and is not sensitive to grain size [47]. It was reported that β phase has the lowest Young's modulus in titanium phases, α'' phase has modulus lower than α phase and the phase with the highest modulus is ω phase [27]. The observation from the SLM produced titanium and its alloys parts are in agreement with the reported results. TiTa samples have the lowest Young's modulus, as only β phase is present, followed by commercially pure titanium (with α phase) samples. Ti6Al4V (with $\alpha' + \beta$ phase) samples have the highest Young's modulus. This observation is also in agreement with findings from other β titanium alloys [48]. In addition, the TiTa specimens have higher ductility, shown by the higher elongation at yield, than Ti6Al4V. However, the higher ductility is a tradeoff for lower yield strength, which is sensitive to size and morphology of the micro-structures [47]. Higher ductility is due to the absence of strain hardening in TiTa alloy. Strain hardening occurs in Ti6Al4V due to the presence of α' martensitic phase, which does not exist in the TiTa alloy.

The differences in microstructure between the materials also translate to differences in microhardness values as shown in
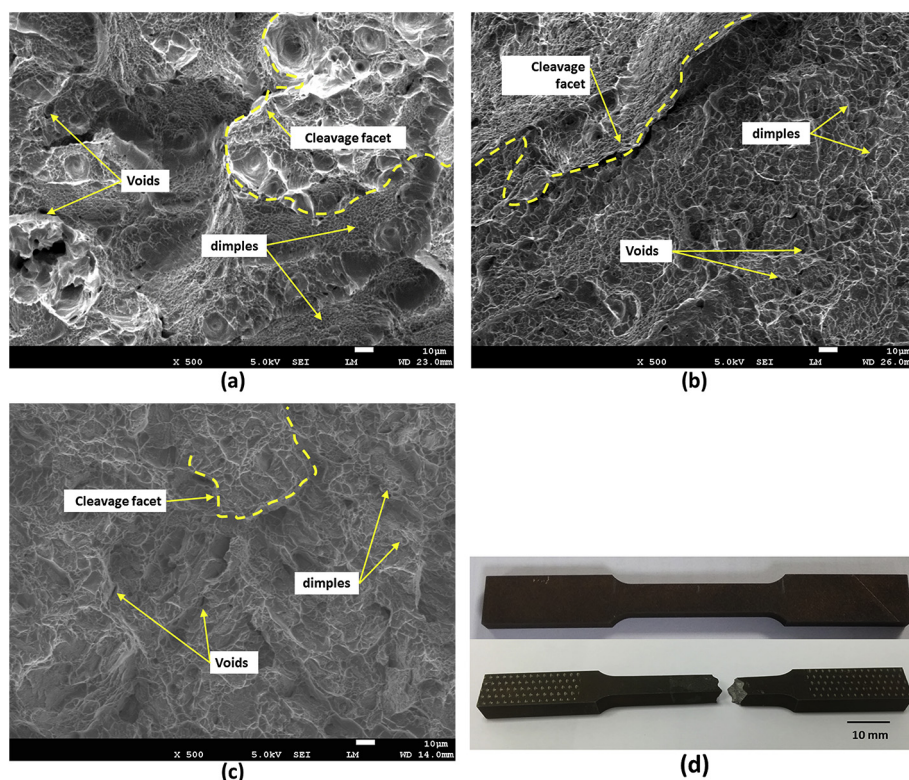
Fig. 17. Fracture surfaces after tensile test (a) TiTa (b) Ti6Al4V (c) commercially pure titanium samples and (d) samples of tensile test coupon before and after fracture.

Table 8
Comparison of properties of TiTa alloy obtained by SLM and arc melting.

Method	Phase present	Young's modulus (GPa)	Ultimate tensile strength (MPa)	Yield strength (MPa)	Elongation (%)	Reference
SLM	β	75.77 ± 4.04	924.64 ± 9.06	882.77 ± 19.60	11.72 ± 1.13	This work
Arc melting	α"	88	530	375	25	[42,43]

Table 7. There is insignificant difference between the microhardness values for the xy plane and yz plane for the TiTa, Ti6Al4V and commercially pure titanium. The random grain orientations without any preferred grain orientation due to the scanning strategy which involves the laser beam moving backwards and forwards, results in similar microhardness values in the two planes.

The fracture surfaces after tensile tests for the materials were investigated using FESEM, as shown in Fig. 17.

All specimens fractured after neck creation. The fracture surfaces confirmed the ductility of the three materials. At microscopic level, they exhibited features showing mixed mode of ductile and brittle fracture. The fractures surfaces showed a combination of ductile dimples and void indicating ductile failures as well as cleavage facets that consisted of flat planes with small atomic steps indicating brittle fracture. The fractures were proceeded predominantly by ductile intragranular fracture mode with dimple-like morphology. As can be seen from Fig. 17(a) the fracture surface of TiTa is covered by very fine dimples of about $2-5$ µm, shown by the brighter lines in the FESEM image. This was compared to the Ti6Al4V which shows larger dimples of about $5-10$ µm. The dimple size is indicative of the fracture energy during the fracture. Ductile fracture was more dominant in TiTa compared to commercially pure titanium, as observed from the smaller cleavage facets and planes on the fracture surface of commercially pure titanium. This could be attributed to the presence of the β phase that is more ductile than the α phase. The higher amount of deep and fine ductile dimples in fracture surface of the TiTa specimen also represents higher ductility of the TiTa alloy.

In addition, the mechanical properties of TiTa obtained from SLM is compared to the alloy with same composition obtained by arc melting in previous works conducted by Zhou et al., and the mechanical properties are summarized in Table 8 [49,50].

TiTa alloy obtained from SLM is able to achieve a higher strength to modulus ratio compared to arc melting. This is due to the rapid solidification and cooling that occurs during the SLM process. The rapid solidification and cooling results in smaller grains in microstructure which leads to higher strengths.

4. Conclusions

The ability of SLM to fabricate TiTa alloy was demonstrated in this research. Tantalum was selected as a potential alloying element based on its ability to stabilize the β phase in the TiTa alloy as well as lowering the Young's modulus. A lower Young's modulus is desirable to reduce stress shielding in biomedical implants. Based on specific applications, the alloy content can be altered to reduce the tantalum particles content or heat treatment can be done to induce the required microstructures and mechanical properties.

The key findings of this research include:

1) TiTa alloy could be fabricated successfully using SLM, demonstrating the SLM capability to process powder mixtures of different materials apart from pre-alloyed powders.
2) TiTa alloy processed by SLM was shown to consist only of β phase due to tantalum stabilizing effect of the phase after rapid solidification

3) Incomplete melting of the larger tantalum particles caused dispersed tantalum particles in the matrix formed by the fully melted titanium and small sized tantalum.
4) TiTa part showed a combination of high strength and lower Young's modulus as compared to commercially pure titanium and Ti6Al4V parts.

References

[1] C.K. Chua, K.F. Leong, 3D Printing and Additive Manufacturing: Principles and Applications, fourth ed., World Scientific Publishing Co. Pte. Ltd, Singapore, 2014.

[2] Z.H. Liu, D.Q. Zhang, S.L. Sing, C.K. Chua, L.E. Loh, Interfacial characterization of SLM parts in multi-material processing: metallurgical diffusion between 316L stainless steel and C18400 copper alloy, Mater. Charact. 94 (2014) 116–125.

[3] S.L. Sing, W.Y. Yeong, C.K. Chua, F.E. Wiria, Z.H. Liu, D.Q. Zhang, B.Y. Tay, Classical Lamination Theory Applied on Parts Produced by Selective Laser Melting, High Value Manufacturing: Advanced Research in Virtual and Rapid Prototyping, 2013, pp. 77–82.

[4] J.F. Sun, Y.Q. Yang, D. Wang, Mechanical properties of a Ti6Al4V porous structure produced by selective laser melting, Mater. Des. 49 (2013) 545–552.

[5] L. Thijs, M.L. Montero Sistiaga, R. Wauthle, Q. Xie, J.-P. Kruth, J. Van Humbeeck, Strong morphological and crystallographic texture and resulting yield strength anisotropy in selective laser melted tantalum, Acta Mater. 61 (2013) 4657–4668.

[6] S.L. Sing, J. An, W.Y. Yeong, F.E. Wiria, Laser and electron-beam powder-bed additive manufacturing of metallic implants: a review on processes, materials and designs, J. Orthop. Res. (2015), http://dx.doi.org/10.1002/jor.23075.

[7] K. Kunze, T. Etter, J. Grässlin, V. Shklover, Texture, anisotropy in microstructure and mechanical properties of IN718LC alloy processed by selective laser melting (SLM), Mater. Sci. Eng. A 620 (2015) 213–222.

[8] Q. Wei, L. Shuai, C. Han, W. Li, L. Cheng, L. Hao, Y. Shi, Selective laser melting of stainless-steel/nano-hydroxyapatite composites for medical applications: microstructure, element distribution, crack and mechanical properties, J. Mater. Process. Technol. 222 (2015) 444–453.

[9] K.G. Prashanth, H. Shakur Shahabi, H. Attar, V.C. Srivstava, N. Ellendt, V. Uhlenwinkel, J. Eckert, S. Scudino, Production of high strength Al85Nd8-Ni5Co2 alloy by selective laser melting, Addit. Manuf. 6 (2015) 1–5.

[10] D. Hu, Y. Wang, D. Zhang, L. Hao, J. Jiang, Z. Li, Y. Chen, Experimental investigation on selective laser melting of bulk net-shape pure magnesium, Mater. Manuf. Process. 30 (11) (2015) 1298–1304.

[11] W.Y. Yeong, C.Y. Yap, M. Mapar, C.K. Chua, State-of-the-art Review on Selective Laser Melting of Ceramics, High Value Manufacturing: Advanced Research in Virtual and Rapid Prototyping, 2013, pp. 65–70.

[12] D. Dai, D. Gu, Tailoring surface quality through mass and momentum transfer modeling using a volume of fluid method in selective laser melting of TiC/AlSi10Mg powder, Int. J. Mach. Tools Manuf. 88 (2015) 95–107.

[13] P. Yuan, D. Gu, Molten pool behaviour and its physical mechanism during selective laser melting of TiC/AlSi10Mg nanocomposites: simulation and experiments, J. Phys. D Appl. Phys. 48 (2015).

[14] H. Attar, K.G. Prashanth, A.K. Chaubey, M. Calin, L.C. Zhang, S. Scudino, J. Eckert, Comparison of wear properties of commerically pure titanium prepared by selective laser melting and casting processes, Mater. Lett. 142 (2015) 38–41.

[15] G. Kasperovich, J. Hausmann, Improvement of fatigue resistance and ductility of Ti6Al4V processed by selective laser melting, J. Mater. Process. Technol. 220 (2015) 202–214.

[16] S.L. Sing, L.P. Lam, D.Q. Zhang, Z.H. Liu, C.K. Chua, Interfacial characterization of SLM parts in multi-material processing: intermetallic phase formation between AlSi10Mg and C18400 copper alloy, Mater. Charact. 107 (2015) 220–227.

[17] H. Tan, J. Chen, F. Zhang, X. Lin, W. Huang, Microstructure and mechanical properties of laser solid formed Ti-6Al-4V from blended elemental powders, Rare Metal Mater. Eng. 38 (2009) 574–578.

[18] D. Gu, Y.-C. Hagedorn, W. Meiners, K. Wissenbach, R. Poprawe, Selective laser melting of in-situ TiC/Ti5Si3 composites with novel reinforcement architecture and elevated performance, Surf. Coat. Technol. 205 (2011) 3285–3292.

[19] D. Gu, W. Meiners, Microstructure characteristics and formation mechanisms of in situ WC cemented carbide based hardmetals prepared by selective laser melting, Mater. Sci. Eng. A 527 (2010) 7585–7592.

[20] D. Gu, G. Meng, C. Li, W. Meiners, R. Poprawe, Selective laser melting of TiC/Ti bulk nanocomposites: influence of nanoscale reinforcement, Scr. Mater. 67 (2012) 185–188.

[21] B. Vrancken, L. Thijs, J.-P. Kruth, J. Van Humbeeck, Microstructure and me-
     chanical properties of a novel β titanium metallic composite by selective laser
     melting, Acta Mater. 68 (2014) 150—158.
[22] E. Sallica-Leva, A.L. Jardini, J.B. Fogagnolo, Microstructure and mechanical
     behavior of porous Ti-6Al-4V parts obtained by selective laser melting,
     J. Mech. Behav. Biomed. Mater. 26 (2013) 98—108.
[23] L. Facchini, E. Magalini, P. Robotti, A. Molinari, S. Höges, K. Wissenbach,
     Ductility of a Ti-6Al-4V alloy produced by selective laser melting of prealloyed
     powders, Rapid Prototyp. J. 16 (2010) 450—459.
[24] L.E. Murr, S.A. Quinones, S.M. Gaytan, M.I. Lopez, A. Rodela, E.Y. Martinez,
     D.H. Hernandez, E. Martinez, F. Medina, R.B. Wicker, Microstructure and
     mechanical behavior of Ti-6Al-4V produced by rapid-layer manufacturing, for
     biomedical applications, J. Mech. Behav. Biomed. Mater. 2 (2009) 20—32.
[25] B. Vrancken, L. Thijs, J.-P. Kruth, J. Van Humbeeck, Heat treatment of Ti6Al4V
     produced by selective laser melting: microstructure and mechanical proper-
     ties, J. Alloys Compd. 541 (2012) 177—185.
[26] L. Thijs, F. Verhaeghe, T. Craeghs, J. Van Humbeeck, J.-P. Kruth, A study of the
     microstructural evolution during selective laser melting of Ti-6Al-4V, Acta
     Mater. 58 (2010) 3303—3312.
[27] E. Chlebus, B. Kuznicka, T. Kurzynowski, B. Dybala, Microstructure and me-
     chanical behaviour of Ti-6Al-7Nb alloy produced by selective laser melting,
     Mater. Charact. 62 (2011) 488—495.
[28] H. Rotaru, G. Armencea, D. Spîrchez, C. Berce, T. Marcu, D. Leordean, S.G. Kim,
     S.W. Lee, C. Dinu, G. Băciuț, M. Băciuț, In vivo behavior of surface modified
     Ti6Al7Nb alloys used in selective laser melting for custom-made implants. A
     preliminary study, Romanian J. Morphol. Embryol. 54 (2013) 791—796.
[29] P. Szymczyk, A. Junka, G. Ziólkowski, D. Smutnicka, M. Bartoszewicz,
     E. Chlebus, The ability of S.aureus to form biofilm on the TI-6Al-7Nb scaffolds
     produced by selective laser melting and subjected to the different types of
     surface modifications, Acta Bioeng. Biomech. 15 (2013) 69—76.
[30] A. Morita, H. Fukui, H. Tadano, S. Hayashi, J. Hasegawa, M. Niinomi, Alloying
     titanium and tantalum by cold crucible levitation melting (CCLM) furnace,
     Mater. Sci. Eng. A 280 (2000) 208—213.
[31] P. Laheurte, F. Prima, A. Eberhardt, T. Gloriant, M. Wary, E. Patoor, Mechanical
     properties of low modulus β titanium alloys designed from the electronic
     approach, J. Mech. Behav. Biomed. Mater. 3 (2010) 565—573.
[32] J. Máleka, F. Hnilicaa, J. Veselýa, B. Smolac, S. Bartáková́d, J. Vaněkd, Micro-
     structure and mechanical properties of Ti-35Nb-6Ta alloy after thermo-
     mechanical treatment, Mater. Charact. 66 (2012) 75—82.
[33] R. Banerjee, S. Nag, J. Stechschulte, H.L. Fraser, Strengthening mechanisms in
     Ti-Nb-Zr-Ta and Ti-Mo-Zr-Fe orthopaedic alloys, Biomaterials 25 (2004)
     3413—3419.
[34] K.A. de Souza, A. Robin, Preparation and characterization of Ti-Ta alloys for
     application in corrosive media, Mater. Lett. 57 (2003) 3010—3016.
[35] L.E. Loh, Z.H. Liu, D.Q. Zhang, M. Mapar, S.L. Sing, C.K. Chua, W.Y. Yeong, Se-
     lective laser melting of aluminium alloy using a uniform beam profile, Virtual

[36] J. Jhabvala, E. Boillat, T. Antignac, R. Glardon, On the effect of scanning stra-
     tegies in the selective laser melting process, Virtual Phys. Prototyp. 5 (2010)
     99—109.
[37] E. Yasa, J. Deckers, J.-P. Kruth, M. Rombouts, J. Luyten, Investigation of sectoral
     scanning in selective laser melting, in: ASME 2010 10th Biennial Conference
     on Engineering Systems Design and Analysis, Istanbul, Turkey, 2010.
[38] D. Doraiswamy, S. Ankem, The effect of grain size and stability on ambient
     temperature tensile and creep deformation in metastable beta titanium alloys,
     Acta Mater. 51 (2003) 1607—1619.
[39] D. Grevey, V. Vignal, I. Bendaoud, P. Erazmus-Vignal, I. Tomashuchuk,
     D. Daloz, P. Sallamand, Microstructure and micro-electrochemical study of a
     tantalum-titanium weld interface, Mater. Des. 87 (2015) 974—985.
[40] C. Kenel, C. Leinenbach, Influence of cooling rate on microstructure formation
     during rapid solidification of binary TiAl alloys, J. Alloys Compd. 637 (2015)
     242—247.
[41] J.I. Qazi, H.J. Rack, Metastable beta titanium alloys for orthopedic applications,
     Adv. Eng. Mater. 7 (2005) 993—998.
[42] D.Q. Zhang, Z.H. Liu, Q.Z. Cai, J.H. Liu, C.K. Chua, Influence of Ni content on
     microstructure of W-Ni alloy produced by selective laser melting, Int. J.
     Refract. Metals Hard Mater. 45 (2014) 15—22.
[43] Y. Zhu, D. Liu, X. Tian, H. Tang, H. Wang, Characterization of microstructure
     and mechanical properties of laser melting deposited Ti-6.5Al-3.5Mo-1.5Zr-
     0.3Si titanium alloy, Mater. Des. 56 (2014) 445—453.
[44] A. Hussien, L. Hao, C. Yan, R. Everson, Finite element simulation of the tem-
     perature and stress fields in single layers build without-supoort in selective
     laser melting, Mater. Des. 52 (2013) 638—647.
[45] L.E. Loh, C.K. Chua, W.Y. Yeong, J. Song, M. Mapar, S.L. Sing, Z.H. Liu,
     D.Q. Zhang, Numerical investigation and an effective modelling on the se-
     lective laser melting (SLM) process with aluminium alloy 6061, Int. J. Heat
     Mass Transf. 80 (2015) 288—300.
[46] D. Gu, Y.-C. Hagedorn, W. Meiners, G. Meng, R.J.S. Batista, K. Wissenbach,
     R. Poprawe, Densification behavior, microstructure evolution, and wear per-
     formance of selective laser melting processed commercially pure titanium,
     Acta Mater. 60 (2012) 3849—3860.
[47] Q. Guo, Y. Zhan, H. Mo, G. Zhang, Aging response of the Ti-Nb system bio-
     materials with β-stabilizing elements, Mater. Des. 31 (2010) 4842—4846.
[48] M. Niinomi, Mechanical properties of biomedical titanium alloys, Mater. Sci.
     Eng. A 243 (1998) 231—236.
[49] Y.-L. Zhou, M. Niinomi, T. Akahori, M. Nakai, H. Fukui, Comparison of various
     properties between titanium-tantalum alloy and pure titanium for biomedical
     applications, Mater. Trans. 48 (2007) 380—384.
[50] Y.L. Zhou, M. Niinomi, T. Akahori, Effects of Ta content on Young's modulus
     and tensile properties of binary Ti-Ta alloys for biomedical applications,
     Mater. Sci. Eng. A 371 (2004) 283—290.